Research Article

Design and Development of g-C_3N_4/ZnO/CdS Ternary Photocatalyst for the Removal of Environmentally Hazardous Organic Dyes under Visible Light

Nagaraju Kottam*
Research Center, Department of Chemistry, Ramaiah Institute of Technology (Autonomous Institute, Affiliated to Visvesvaraya Technological University, Belgaum, Karnataka, India) Bengaluru, Karnataka, India

Koteswara Rao Jammula*, Sagar J. Shivaram, Balaji Adavichambakuru Rajappa and Priyanka Narayanappa
Department of Chemical Engineering, M S Ramaiah Institute of Technology, Karnataka, India

Smrithi Sailaja Prasannakumaran Nair
Department of Applied Sciences, School of Advanced Studies, S-Vyasa Deemed to be University, Karnataka, India

Atthasit Tawai
The Sirindhorn International Thai-German Graduate School of Engineering, Biorefinery and Process Automation Engineering Center (BPAEC), King Mongkut's University of Technology North Bangkok, Bangkok, Thailand

* Corresponding author. E-mail: nagaraju@msrit.edu, koteswararao@msrit.edu DOI: 10.14416/j.asep.2024.11.008
Received: 10 September 2024; Revised: 19 October 2024; Accepted: 5 November 2024; Published online: 21 November 2024

Abstract
The processing of wastewater has emerged as a primary focus of research owing to the unavailability of clean water to satisfy the current population's needs. In this work, a ternary nano-photocatalyst, g-C_3N_4/ZnO/CdS exhibiting visible light activity has been fabricated via a dual-step process that involved a pyrolytic transformation of urea to g-C_3N_4 subsequently followed by the solid state mechanochemical method to fabricate g-C_3N_4/ZnO/CdS. The synthesized nanomaterial underwent characterization using advanced techniques such as XRD, FTIR, FE-SEM/EDAX and UV-DRS techniques. The decomposition of Indigo Carmine dye was performed under the illumination of visible light, resulting in 99.6% degradation using a 50-mg photocatalytic dosage. Kinetic studies indicate that the photodegradation process followed pseudo-first-order where the phenomenon of adsorption adhered to the Langmuir–Hinshelwood model. This work attempted the generation of a multi pathway of electron migration by combining more than one Type-II heterojunction, which can effectively delay the electron-carrier recombination.

Keywords: Dye degradation, Kinetics, Photocatalysis, Type II heterojunction, Visible light, Wastewater

1 Introduction

Water pollution is a significant environmental issue characterized by the contamination of water bodies owing to the infusion of toxic substances. The pollution can result in detrimental impacts on marine habitats, human well-being and the global ecological balance. A significant focus of the research community is directed towards lingering poisonous pollutants present in freshwater ecosystems [1]–[3]. Due to industrial expansion, a considerable quantity of organic dyes has been released into the environment's water bodies. Out of which, a few of them have shown mutagenic and carcinogenic properties. Reports indicate that the extensive utilization of both antibiotic medications and organic dyes poses a significant menace to the ecosystem. Hence, the urgent need arises for the

elimination of these contaminants from natural water sources. The examination of various treatment methods has revealed the partial elimination of toxic contaminants, indicating their incomplete removal as well as the detection of secondary pollutants [4]–[6]. However, photocatalysis serves as an impactful and streamlined approach for purging organic contaminants from wastewater. The commercially accessible TiO_2 photocatalyst with an energy gap of approximately 3.2 eV exhibits activity solely on exposure to ultraviolet rays. This is the reason why photocatalyst exhibits limited photoactivity when subjected to visible light. In general, ZnO photocatalysts are only active in ultraviolet rays, which comprise approximately 5% of solar light [7], [8]. Normally, nanostructured photocatalysts exhibit higher photo-activity compared to bulk materials. However, it is generally recognized that charge-carrier recombination constitutes a significant limitation contributing to the reduced effectiveness of synthesized photocatalysts [9]–[13]. As a result, the development of photocatalysts active under visible light holds a greater promise than the production of traditional TiO_2 or ZnO photocatalysts. Several photocatalysts driven by solar light, such as g-C_3N_4, MoS_2 and Ag_3PO_4 have been reported [14]–[16].

To broaden light absorption within the visible spectrum while mitigating the challenge of heightened recombination, metal-semiconductor or semiconductor-semiconductor heterojunctions offer a viable solution. A crucial aspect to contemplate in the design of heterojunctions for enhanced photocatalytic performance is the alignment of band edges [17]–[20]. The alignment and bending of bands can significantly rely on the sizes of particles and their positioning relative to one another. Vibrations based on facets have also been noted in band bending, influencing the movement of charges throughout interfaces of various contacting planes and thus impacting photocatalytic performance [21], [22]. Moreover, band bending manifests not only at the junctions between distinct materials or dissimilar phases of crystal made of identical material but also between larger and smaller particles of the identical material possessing the similar crystal structure. In such instances, the variance in facade band bending results in the generation of an electric field, facilitating the separation of charge carriers. Heterojunction semiconductor photocatalysts such as NiO/g-C_3N_4, CeO_2-AgI, CdS/MoS_2, g-C_3N_4/Bi_2WO_6, $ZnIn_2S_4$-In_2O_3, In_2S_3/Cd, In_2S_4 nanotubes, Ag_2O/Bi_5O_7I, g-$C_3N_4/ZnIn_2S_4$, ZnS/g-C_3N_4, g-C_3N_4/phosphorene etc. have been documented by different researchers [23]. However, additional improvements are still required to augment visible light absorptivity and enhance the segregation of charge carriers. To accomplish this objective, researchers have explored particular categories of heterojunctions, such as Z-schemes and plasmonic photocatalysts to mitigate recombination losses and harness plasmonic effects, respectively.

A formation of ternary Type–II heterojunctions based on Z-scheme photocatalysis is considered advantageous once compared with traditional Z-scheme photocatalysts. A ternary system means three components are working together. In this case, three different semiconductors are combined into a Type-II heterojunction configuration. The ternary structure provides more pathways for charge transfer and separation, enhancing the ability to utilize light energy efficiently. The third material can help to extend the absorption range into the visible light spectrum, improves charge separation, or acts as a bridge between the other two materials, facilitating better electron flow and further reducing recombination. The strategic combination of materials in a ternary system can result in a more stable photocatalyst compared to some traditional Z-scheme structures, which might degrade faster under light [24], [25]. There is an intriguing opportunity to leverage the distinct band potentials of these single semiconductor counterparts to facilitate charge separation by creating heterostructures between them. This approach aims to significantly enhance the performance of photocatalytic activity (PCA) in these heterostructures [26].

This work reports the successful design of ternary Type–II heterojunctions using g-CN/ZnO/CdS nanophotocatalysts via a two-step synthesis strategy to investigate its efficiency in the breakdown of Indigo Carmine dye (IC). IC dye is a synthetic dye that finds widespread application as a food colorant, pH indicator in chemical laboratories, medical diagnosis procedures, and textile industries, etc. At high concentrations, IC dye proves to be toxic to aquatic life potentially leading to a decrease in biodiversity. It can lead to a reduction in the amount of dissolved oxygen in water bodies, which is in turn crucial for the survival of aquatic life. Hence, degradation of IC dye using visible light mediated photocatalysis is highly relevant.

2 Materials and Techniques

2.1 *Materials*

The subsequent chemicals have been used for this study and they are employed as purchased without further purification. Urea (CH_4N_2O), zinc chloride ($ZnCl_2$), thiourea (CH_4N_2S) and cadmium nitrate ($Cd(NO_3)_2.4H_2O$ have been purchased from Sigma Aldrich. Indigo carmine, hydrochloric acid (HCl) and sodium hydroxide (NaOH) have been purchased from Sisco Research Laboratories.

2.2 *Techniques/Methods*

2.2.1 Fabrication of graphitic carbon nitride

The graphitic carbon nitride (g-C_3N_4) was obtained by the pyrolysis of extra pure urea in the muffle furnace for three hours and heated at the rate of 2 °C min^{-1} and maintained at 500 °C under air tight conditions. The obtained samples were allowed to reach room temperature. The synthesized product was ground well into fine powder and weighed.

2.2.2 Fabrication of g-C_3N_4/ZnO /CdS composite

The prepared g-C_3N_4 was weighed and 5 g of this sample was transferred into a mortar. Along with g-C_3N_4, 1 g of zinc chloride ($ZnCl_2$), 1 g of cadmium nitrate tetrahydrate ($CdN_2O_6.4H_2O$) and 1 g of thiourea were mixed together using the mortar and pestle until a fine powder is obtained. The obtained product was transferred into a silica crucible and heated in a high temperature furnace maintained at 300 °C for 4 h. The obtained product was cooled to room temperature. The desired composite of yellow-colored g-C_3N_4/ZnO /CdS was obtained.

2.2.3 Dye degradation studies

A freshly prepared 5 ppm dye solution (100 mL) was transferred into a clean 250 mL beaker. The initial absorbance of the solution was recorded using a Shimadzu UV–VIS 1800 spectrophotometer. Subsequently, 25 mg of the g-C_3N_4/ZnO/CdS composite catalyst was introduced into the dye solution, and the mixture was stirred for 10 min in the dark to ensure the proper adsorption. The dye concentration was then measured at 15-min intervals during light irradiation using a UV-visible spectrophotometer, following the removal of the catalyst by centrifugation. The same procedure was followed for different catalytic dosages.

3 Results and Discussion

3.1 *Characterisation of the photocatalyst*

The PXRD of g-C_3N_4 and g-C_3N_4/ZnO/CdS are depicted in Figure 1. The characteristic peaks of (274) (345) (452) (544) and the corresponding diffraction peaks were observed at these 2θ values 20.04°, 22.66°, 26.61°, 26.61° and 30.01° values are observed that have a good agreement with the data of g-C_3N_4 as per the previous reports [27], [28].

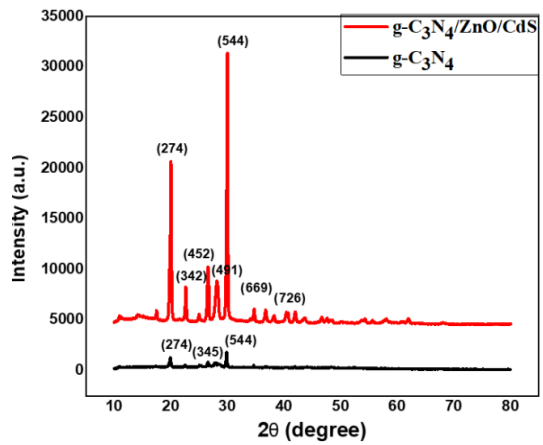

Figure 1: XRD pattern obtained for g-C_3N_4.

The result obtained for the XRD studies of the photocatalyst, g-C_3N_4/ZnO/CdS clearly shows a few additional peaks when compared with the XRD pattern obtained for g-C_3N_4. The peaks corresponding to 29.85° and 34.62° corresponds to the (491) and (669) planes, respectively, of wurtzite phase of ZnO. Also, the peaks obtained at 28.05° and 36.72° indicates the presence of (101) and (110) planes of CdS hexagonal wurtzite phase [29]. The sharp peak indicate the crystalline nature of the synthesised photocatalyst and confirms the formation of g-C_3N_4/ZnO/CdS [30].

The vibrational spectroscopic (FTIR) studies of the g-C_3N_4/ZnO/CdS photocatalyst (Figure 2) show the typical Zn-O vibrational band at 500 cm^{-1} while a medium absorption band around 650 cm^{-1} corresponding to the presence of Cd-S bonds. The multiple bands dominated around 1100–1700 cm^{-1} corresponds to the bands originating from g-C_3N_4 owing to the characteristic vibrations of aromatic – CN

heterocycles [31]. To accomplish the optical characteristic evaluation of g-C_3N_4 and the synthesized photocatalyst, UV-visible diffuse reflectance spectroscopic analysis is carried out and the obtained spectrum is shown in Figures 3 and 4, respectively. The broad spectrum as seen in Figure 4 suggested the enhanced visible range absorptivity of the synthesized g-C_3N_4/ZnO/CdS as compared with the limited UV-visible absorption range exhibited by g-C_3N_4.

Scanning electron microscopy was employed for the examination of surface morphology of g-C_3N_4/ZnO/CdS. The monodispersed spherical-like morphology of g-C_3N_4/ZnO/CdS is evident (Figure 5). Additionally, the elemental composition of the sample acquired from EDAX confirms the presence of elements such as C, N, O, Cd, S and Zn. This in turn supports the generation of g-C_3N_4/ZnO/CdS nanocomposite (Figure 6 and Table 1).

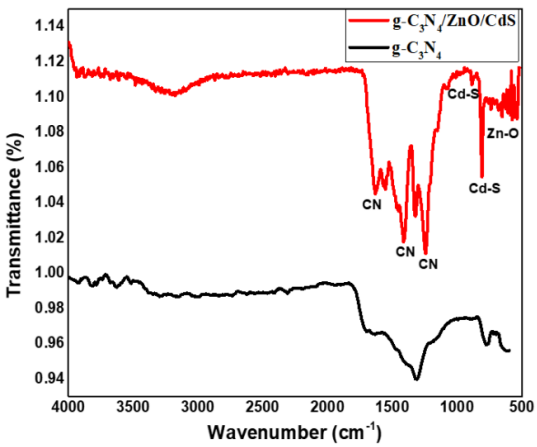

Figure 2: FTIR spectra obtained for g-C_3N_4 and g-C_3N_4/ZnO/CdS.

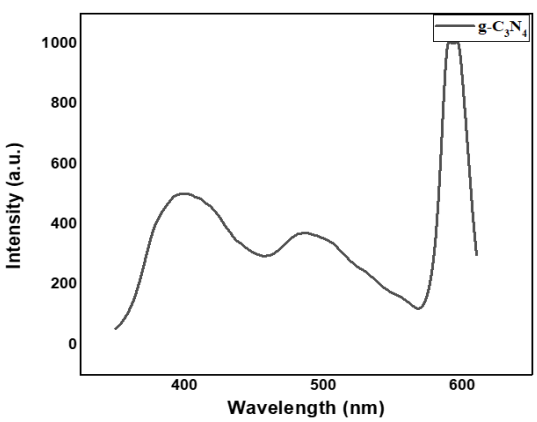

Figure 3: UV-DRS spectrum obtained for g-C_3N_4.

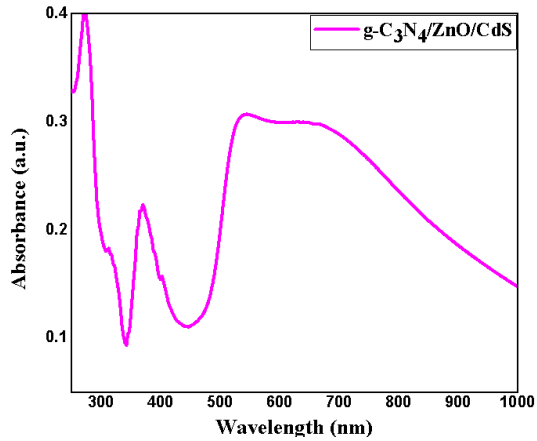

Figure 4: UV-DRS spectrum obtained for g-C_3N_4/ZnO/CdS.

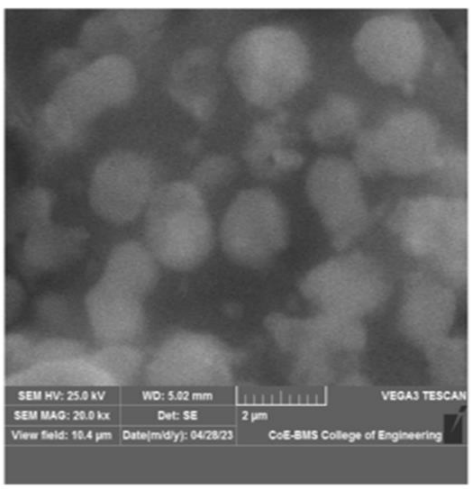

Figure 5: SEM image spectra of g-C_3N_4/ZnO/CdS.

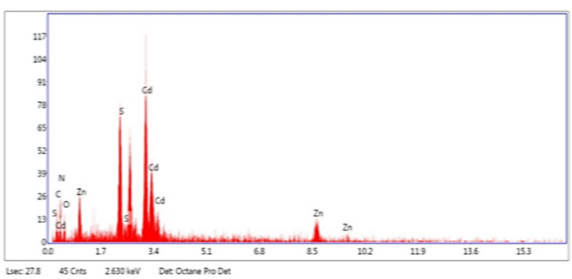

Figure 6: EDAX spectrum of g-C_3N_4/ZnO/CdS.

Table 1: Consolidated elemental composition from EDAX spectrum.

Element	Weight %	Atomic %
C	15.46	28.03
N	24.20	37.62
O	14.54	19.79
S	9.11	6.19
Cd	27.57	5.34
Zn	9.13	3.04

3.2 *Visible light assisted photocatalytic breakdown of indigo carmine dye*

The degradation studies using 100 mL of Indigo Carmine (IC) as a model pollutant at a concentration of 5 ppm was assessed using the g-C_3N_4/ZnO/CdS photocatalyst under neutral conditions in the absence and the presence of the photocatalyst under visible light (Figures 7 and 8). It was noted that the decomposition of IC dye under neutral conditions is found to be 99.6 % after the irradiation of light for 105 min for 50 mg catalytic dosage of g-C_3N_4/ZnO/CdS (Figure 7). This enhanced degradation could be owing to the delayed charge-carrier recombination owing to the type-II heterojunction fabricated using the semiconductors of varying band edge positions.

On the other side in the absence of the catalyst, the degradation was found to be less efficient in achieving the degradation of IC dye after 80 min of irradiation of visible light (Figure 8). In order to know the optimum catalytic dosage of the ternary photocatalyst in the degradation process, the same experiment was conducted using 25 mg, 75 mg and 100 mg of the g-C_3N_4/ZnO/CdS dosage. Both the 25 mg and 75 mg dosages have resulted in slightly less photocatalytic degradation efficiency when compared with the 50 mg dosage. This result confirms it as the optimum catalytic dosage for 100 mL of 5 ppm dye concentration (Figure 9).

An investigation has been carried out using different radical scavengers namely benzoquinone, ammonium oxalate and isopropyl alcohol of 1 mmolL^{-1} concentration to reveal the active moieties involved in the light assisted catalytic process. The scavengers have been added along with the photocatalyst under the optimized conditions and the findings are consolidated in Figure 10. It has been noted that the addition of ammonium oxalate has considerably reduced the degradation efficiency which implies that the superoxide anion radical executes a significant function in the degradation procedure than the hydroxyl radicals and the holes [32], [33].

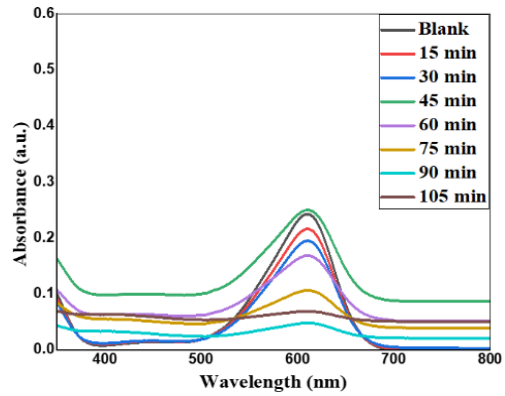

Figure 7: Degradation of IC dye using 50 mg of g-C_3N_4/ZnO/CdS in neutral conditions.

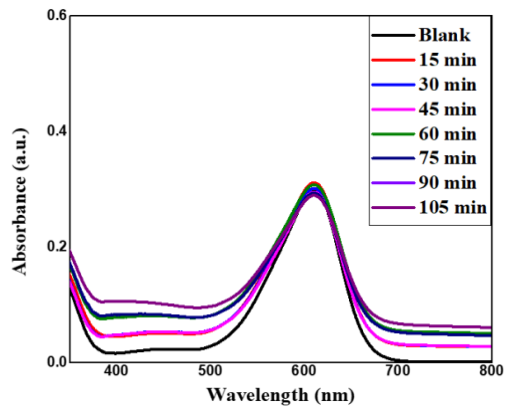

Figure 8: Degradation of IC dye without catalyst in neutral conditions.

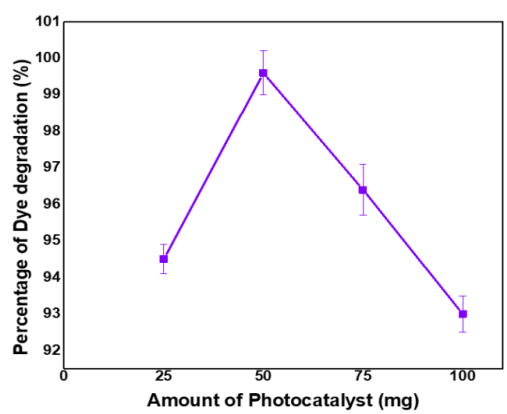

Figure 9: Plot of percentage of dye degradation against various catalytic dosages.

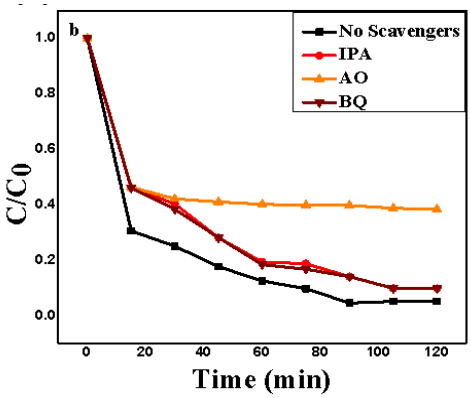

Figure 10: Results of radical trapping experiment.

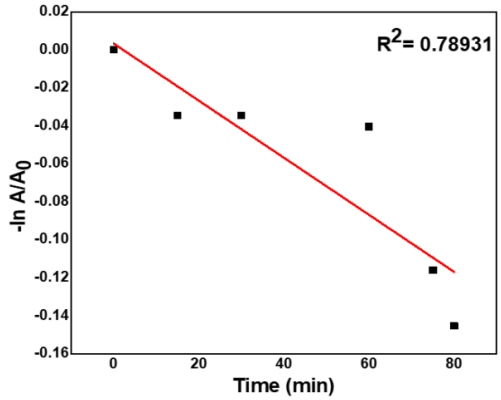

Figure 11: Pseudo-first-order plot for a neutral medium of dye solution using 50 mg catalytic dosage of g-C_3N_4/ZnO /CdS.

3.3 *Study on the kinetics of the degradation process*

The chemical kinetics involved in the photocatalytic reaction; the decomposition of Indigo carmine dye using g-C_3N_4/ZnO/CdS photocatalyst, were examined to gain an understanding of the photodegradation mechanism and to evaluate the practicality and effectiveness of utilizing this method for dye treatment. The pseudo-first-order reaction can be expressed by the subsequent Equation (1):

$$\ln\left(\frac{a}{a0}\right) = -K_{app}\, t \qquad (1)$$

where K_{app} is the degradation rate constant and t is the time of irradiation [34]–[36].

The plot of the negative natural logarithm of (A/A_0) against time, *t* for the reaction in the neutral medium is shown in Figure 11. A linearity between - ln (A/A_0) and *t* was established for the optimized value of 50 mg photocatalyst backing the inference that the photo-degradation process adheres to the kinetics of pseudo-first-order for the concerning concentration of the organic dye. The values for K_{app} were computed from the slopes of ln (A/A_0) against the time plot and were found to be –0.0015 min^{-1} and R^2 = 0.78931. The -ln(A/A_0) versus t plot for 100 mg of the photocatalytic loading in a neutral medium is shown in Figure 12.

An acquired linear association between - ln(A/A_0) and *t* reinforces the inference that the photodegradation process adheres to pseudo-first-order kinetics concerning the concentration of dye. The values for K_{app} were computed from the graphical slopes of -ln(A/A_0) vs. time plot. K_{app} value was found to be –0.01306 min^{-1} and R^2 = 0.88681 (Table 2).

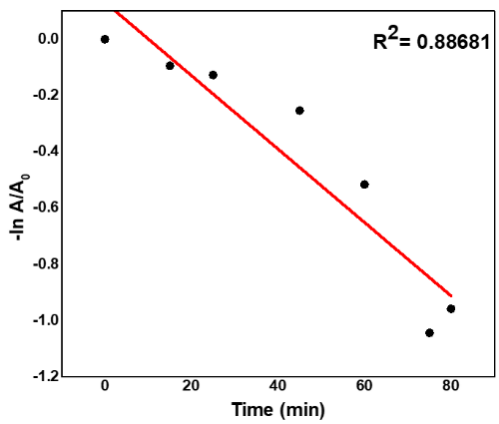

Figure 12: Pseudo-first-order plot for a neutral medium of dye solution using 100 mg catalyst loading of g-C_3N_4 /ZnO /CdS.

Table 2: K_{app} value and R-Square values for 50 mg and 100 mg catalyst.

Catalyst dosage (mg)	K_{app} values (min^{-1})	R^2 values
50	−0.0015	0.7893
100	−0.0136	0.8868

The suggested photocatalytic behavior of g-C_3N_4/ZnO/CdS through multi-routes enhances the possibility of the ejection of electrons towards conduction bands rather than the recombination as depicted in Figure 13. Considering the lower conduction band edge positions, the band of conduction for g-C_3N_4 is rich in electrons when compared with their other counterparts. At the same time, the valence band of CdS is considered to have more holes owing to its higher energy level position

[37]. Hence, it can be assumed that the electron abundant conduction band of g-C_3N_4 acts as the central platform for the pathway of reductive degradation whereas the valence band of the CdS entity behaves as the oxidative pathway of degradation. Overall enhancement in the degradation efficiency is owing to the synergistic effect of the Type-II heterojunctions combined here, which already persists in the individual binary composites.

There were many attempts employed to enhance the photocatalytic characteristics of g-C_3N_4-based photocatalysts through the investigation of the fabrication of numerous g-C_3N_4 based photocatalytic heterostructures such as CdS/g-C_3N_4, CdS/ZnO, SnO_2/g-C_3N_4, which all finally resulted in the slightly enhanced photodegradation based on the characteristic synergetic photocatalytic mechanism of the binary composite [38]–[40]. The current work stands unique as the enhanced degradation of indigo carmine was achieved via the formation of a unique ternary composite that showed promising and competing results when compared to those reported in the literature.

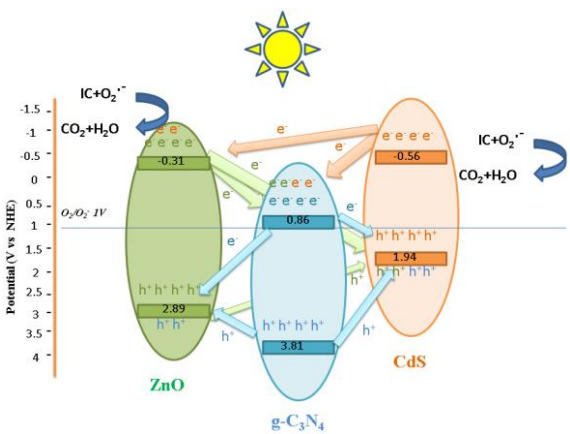

Figure 13: Suggested mechanism for the photocatalytic degradation of Indigo carmine dye using g-C_3N_4/ZnO/CdS photocatalyst.

4 Conclusions

This study reports the generation of g-C_3N_4 by the pyrolytic treatment of urea at 500 °C followed by the fabrication of g-C_3N_4/ZnO/CdS nanoparticles by the calcination of the mixture of the calculated quantities of g-C_3N_4, $ZnCl_2$ and $CdNO_3.4H_2O$ in presence of thiourea at 300 °C for 4 h. The structural configuration and morphological form of these nanoparticles were investigated using XRD, FTIR, UV-DRS and SEM-EDX analysis. The composite photocatalysts (g-C_3N_4/ZnO/CdS) exhibited enhanced photocatalytic activity of 99.6% under the visible light irradiation and the highest degree of degradation for indigo carmine dye was observed under 50 mg catalytic dosage. The complete breakdown of indigo carmine dye in a neutral medium was achieved after 105 min of visible light irradiation. The photocatalytic dye degradation was observed to follow pseudo-first-order kinetics. Therefore, the nanoparticle, g-C_3N_4/ZnO/CdS demonstrates its effectiveness as a photocatalyst in purifying industrial wastewater by removing organic pollutants, thereby mitigating significant environmental hazards. This work elucidates the construction of multiple Type-II-based hetero-junctions in a single component which proves as a key strategy for the enhancement of the resultant photocatalytic performance.

Acknowledgement

Authors wish to acknowledge the management of Ramaiah Institute of Technology, Bengaluru for providing the facilities via Centre for Advanced materials Technology.

Author Contributions

N.K.: conceptualisation, methodology, data curation and reviewing; K.R.J.: research design, methodology, editing; S.J.S.: research design, methodology, editing; S.P.S.: writing original draft, data analysis and editing; B.A.R.: methodology, assisting manuscript preparation, data curation; P.N.: methodology, manuscript refinement, editing, data curation; A.T.: Manuscript refinement, editing, data curation. All authors have read and agreed to the published version of manuscript

Conflicts of Interest

Authors declare no conflicts of interest.

References

[1] C. Buzea, I. I. Pacheco, and K. Robbie, "Nanomaterials and nanoparticles: sources and toxicity," *Biointerphases*, vol. 2, pp. 17–71, 2007, doi: 10.1116/1.2815690.

[2] P. Su, H. Liu, and Z. Jin, "Hierarchical $Co_3(PO_4)_2$/CuI/g-C $_n$ $H_{2\,n-2}$ S-Scheme heterojunction

for efficient photocatalytic hydrogen evolution," *Inorganic Chemistry*, vol. 60, pp. 19402–19413, 2021, doi: 10.1021/acs.inorgchem.1c03223.

[3] D. Dutta, S. Arya, and S. Kumar, "Industrial wastewater treatment: Current trends, bottlenecks, and best practices," *Chemosphere*, vol. 285, 2021, Art. no. 131245, doi: 10.1016/j.chemosphere.2021.131245.

[4] A. Habibi-Yangjeh, S. Asadzadeh-Khaneghah, S. Feizpoor, and A. Rouhi, "Review on heterogeneous photocatalytic disinfection of waterborne, airborne, and foodborne viruses: Can we win against pathogenic viruses?," *Journal of Colloids and Interface Science*, vol. 580, pp. 503–514, 2020, doi: 10.1016/j.jcis.2020.07.047.

[5] T. Xiao, Z. Tang, Y. Yang, Y. L. Tang, Y. Zhou and Z. Zou, "In situ construction of hierarchical WO_3/g-C_3N_4 composite hollow microspheres as a Z-scheme photocatalyst for the degradation of antibiotics," *Applied Catalysis B: Environmental*, vol. 220, pp. 417–428, 2018, doi: 10.1016/j.apcatb.2017.08.070.

[6] A. B. Djurišić, Y. He, and A. M. Ng, "Visible-light photocatalysts: Prospects and challenges," *Applied Materials*, vol. 8, 2020, Art. no. 030903, doi: 10.1063/1.5140497.

[7] M. H. Huang, and M. Madasu, "Facet-dependent and interfacial plane-related photocatalytic behaviors of semiconductor nanocrystals and heterostructures", *Nano Today*, vol. 28, 2019, Art. no. 100768, doi: 10.1016/j.nantod.2019.100768.

[8] Y. Bai, Y. Zhou, J. Zhang, X. Chen, Y. Zhang, J. Liu, and C. Li, "Homophase junction for promoting spatial charge separation in photocatalytic water splitting," *ACS Catalysis*, vol. 9, pp. 3242–3252, 2019, doi: 10.1021/acscatal.8b05050.

[9] L. Jiang, X. Yuan, G. Zeng, J. Liang, Z. Wu, and H. Wang, "Construction of an all-solid-state Z-scheme photocatalyst based on graphite carbon nitride and its enhancement to catalytic activity," *Environmental Science: Nano*, vol. 5, pp. 599–615, 2018, doi: 10.1039/C7EN01031A.

[10] E. A. Abdullah, "Band edge positions as a key parameter to a systematic design of heterogeneous photocatalyst", *European Journal of Chemistry*, vol. 10, pp. 82–94, 2019, doi: 10.5155/eurjchem.10.1.82-94.1809.

[11] X. Jia, X. Q. Han, M. Zheng, and H. Bi, "One pot milling route to fabricate step-scheme AgI/I-BiOAc photocatalyst: Energy band structure optimized by the formation of solid solution," *Applied Surface Sciences*, vol. 489, pp. 409–419, 2019, doi: 10.1016/j.apsusc.2019.05.361.

[12] T. Di, Q. Xu, W. Ho, H. Tang, Q. Xiang, and J. Yu, "Review on metal sulphide-based z-scheme photocatalysts," *ChemCatChem*, vol. 11, pp. 1394–1411, 2019, doi: 10.1002/cctc.201802024.

[13] R. Wang, J. Shen, W. Zhang, Q. Liu, M. Zhang, H. T. Zulfiqar, and H. Tang. "Build-in electric field induced step-scheme TiO_2/$W_{18}O_{49}$ heterojunction for enhanced photocatalytic activity under visible-light irradiation," *Ceramic International*, vol. 46, pp. 23–30, 2020, doi: 10.1016/j.ceramint.2019.08.226.

[14] C. Zhang, M. Zhang, Y. Li, and D. Shuai, "Visible-light-driven photocatalytic disinfection of human adenovirus by a novel heterostructure of oxygen-doped graphitic carbon nitride and hydrothermal carbonation carbon," *Applied Catalysis B: Environmental*, vol. 248, pp. 11–21, 2019, doi: 10.1016/j.apcatb.2019.02.009.

[15] Y. Boyjoo, H. Sun, J. Liu, V. K. Pareek, and S. Wang, "A review on photocatalysis for air treatment: From catalyst development to reactor design," *Chemical Engineering Journal*, vol. 310, pp. 537–559, 2017, doi: 10.1016/j.cej.2016.06.090.

[16] Q. Xiang, B. Cheng, and J. Yu, "Graphene-based photocatalysts for solar-fuel generation," *Angewandte Chemie International Edition*, vol. 54, pp. 11350–11366, 2015, doi: 10.1002/anie.201411096.

[17] L. Marzo, S. K. Pagire, O. Reiser, and B. König, "Visible-light photocatalysis: Does it make a difference in organic synthesis?," *Angewandte Chemie International Edition*, vol. 57, pp. 10034–10072, 2018, doi: 10.1002/anie.201709766.

[18] A. Thomas, A. Fischer, F. Goettmann, M. Antonietti, J. O. Müller, R. Schlögl, and J. M. Carlsson, "Graphitic carbon nitride materials: variation of structure and morphology and their use as metal-free catalysts," *Journal of Materials Chemistry*, vol. 18, pp. 4893–4908, 2008, doi: 10.1039/B800274F.

[19] Q. Guo, Y. Xie, X. Wang, S. Lv, T. Hou, and X. Liu, "Characterization of well-crystallized graphitic carbon nitride nanocrystallites via a

benzene-thermal route at low temperatures," *Chemical Physics Letters*, vol. 380, pp. 84–87, 2003, doi: 10.1016/j.cplett.2003.09.009.

[20] X. Chen, L. Zhang, B. Zhang, X. Guo, and X. Mu, "Highly selective hydrogenation of furfural to furfuryl alcohol over Pt nanoparticles supported on g-C_3N_4 nanosheets catalysts in water," *Scientific Reports*, vol. 6, 2016, Art. no. 28558, doi: 10.1038/srep28558.

[21] G. Mamba, and A. K. Mishra, "Graphitic carbon nitride (g-C_3N_4) nanocomposites: A new and exciting generation of visible light driven photocatalysts for environmental pollution remediation," *Applied Catalysis B: Environmental*, vol. 198, pp. 347–377, 2016, doi: 10.1016/ j.apcatb.2016.05.052.

[22] I. Medina-Ramírez, A. Hernández-Ramírez, and M. L. Maya-Trevino, "Synthesis methods for photocatalytic materials," *Photocatalytic Semiconductors: Synthesis, Characterization, and Environmental Applications*, vol. 5, pp. 69–102, 2015, doi: 10.1007/978-3-319-10999-2_3.

[23] Z. Fona, Irwan, A. Setawan, and Adriana, "Review on advance catalyst for biomass gasification," *Applied Science and Engineering Progress*, vol. 17, 2024, Art. no. 7295, doi: 10.14416/j.asep.2024.01.001.

[24] M. Omar, S. Omar, A. Eltaweil, M. Gehan, and F. Nour, "Engineering of ternary photocatalysts nanocomposites based NiS/ZrO_2/CdSfor boosting of photocatalytic degradation of organic pollutants," *Surfaces and Interfaces*, vol. 43, 2023, Art. No. 103606, doi: 10.1016/ j.surfin. 2023.103606.

[25] Y. Bai, S. Zhang, S. Feng, M. Zho, and S. Ma, "The first ternary Nd-MOF/GO/Fe_3O_4 nanocomposite exhibiting an excellent photocatalytic performance for dye degradation" Dalton Transactions, vol. 49, pp. 10745–10754, 2020, doi: 10.1039/D0DT01648A.

[26] G. Prasanth, G. M. Madhu, and N. Kottam, "Combustion assisted synthesis of cuo nanoparticles and structure-property evaluation in nano-cuo polymer composites," *Applied Science and Engineering Progress*, vol. 17, 2024, Art. no. 7259, doi: 10.14416/j.asep. 2023.11.009.

[27] C. L. Perrin, "Linear or nonlinear least-squares analysis of kinetic data?," *Journal of Chemical Education*, vol. 94, pp. 669–672, 2017, doi: 10.1021/acs.jchemed.6b00629.

[28] S. P. Smrithi, N. Kottam, A. Narula, G. M. Madhu, M. Riyaz, and R. Agilan, "Carbon dots decorated cadmium sulphide heterojunction-nanospheres for the enhanced visible light driven photocatalytic dye degradation and hydrogen generation," *Journal of Colloids and Interface Science*, vol. 627, pp. 956–968, 2022, doi: 10.1016/j.jcis.2022.07.100.

[29] S. P. Smrithi, N. Kottam, and B. R. Vergis, "Heteroatom modified hybrid carbon quantum dots derived from *Cucurbita pepo* for the visible light driven photocatalytic dye degradation," *Topics in Catalysis*, vol. 20, pp. 1–12, 2022, doi: 10.1007/s11244-022-01581-x.

[30] P. B. Raja, K. R. Munuswamy, V. Perumal, and M. N. M. Ibrahim, "Nanobioremediations: fundamentals and applications," micro and nanotechnologies, vol.5, pp. 57–83, 2022, doi: 10.1016/B978-0-12-823962-9.00037-4.

[31] S. P. Smrithi, N. Kottam, V. Arpitha, A. Narula, G. N. Anilkumar, and K. R. V. Subrahmanian, "Tungsten oxide modified with carbon nanodots: Integrating adsorptive and photocatalytic functionalities for water remediation," *Journal of Science: Advanced Materials and Devices*, vol. 5, pp. 73–83, 2020, doi: 10.1016/j.jsamd. 2020.02.005.

[32] S. Sharieff, S. Veluturla, N. Kottam, S. P. Smrithi, and R. Singhvi, "Esterification of levulinic acid to butyl levulinate over TiO_2/WO_3/SO_4: optimization and kinetic study," *Biomass Conversion and Biorefineries*, vol. 1, pp. 1–15, 2023, doi: 10.1007/s13399-023-04016-z.

[33] K. Gurushantha, N. Kottam, S. P. Smrithi, M. S. Dharmaprakash, K. Keshavamurthy, S. Meena, and N. Srinatha, "Visible light active WO_3/TiO_2 heterojunction nanomaterials for electrochemical sensor, capacitance and photocatalytic applications," *Catalysis Letters*, vol. 154, pp. 982–993, 2023, doi: 10.1007/s10562-023-04362-7.

[34] B. Archana, N. Kottam, S. P. Smrithi, and K. B. C. Sekhar, "Fabrication of 2D+1D nanoarchitecture for transition metal oxide modified CdS nanorods: A comparative study on their photocatalytic hydrogen-generation efficiency," *Nanotechnology*, vol. 34, pp. 297–302, 2023, doi: 10.1088/1361-6528/acec50.

[35] B.K. Devendra, B. M. Praveen, V. S. Tripathi, G. Nagaraju, B. M. Prasanna, and M. Shashank, "Development of rhodium coatings by

electrodeposition for photocatalytic dye degradation," *Vacuum*, vol. 205, 2022, Art. No. 111460, doi: 10.1016/j.vacuum.2022.111460.

[36] T. Song, C. Xie, K. Matras-Postolek, and P. Yang, "2D Layered g-C_3N_4/WO_3/WS_2 S-Scheme Heterojunctions with Enhanced Photochemical Performance," *Journal of Physical Chemistry C*, vol. 125, pp. 19382–19393, 2021, doi: 10.1021/acs.jpcc.1c06753.

[37] E. M. Hashem, M. A. Hamza, E. Shazly, S. A. Rahman, E. M. Tanany, R. T. Mohamed, and N. K. Allam, "Novel Z-Scheme/Type-II CdS@ZnO/g-C_3N_4 ternary nanocomposites for the durable photodegradation of organics: Kinetic and Mechanic insights," *Chemosphere*, vol. 277, 2021, Art. No. 128730, doi: 10.1016/j.chemosphere.2020.128730.

[38] Y. Xu and W. Zhang, "CdS/g-C_3N_4 hybrids with improved photostability and visible light photocatalytic activity," *European Journal of Inorganic Chemistry*, vol. 10, pp. 1744–1755, 2015, doi: 10.1002/ejic.201403193.

[39] K. A. Adagoke, M. Iqbal, H. Louis, and O. S. Bello, "Synthesis, characterization application of CdS/ZnO nanorod heterostructure for the photodegradation of Rhodamine B dye". *Material Science and Energy Technology*, vol. 2, pp. 329–336, 2019, doi: 10.1016/j.mset.2019.02.008.

[40] G. Prashanth, G. M. Madhu, N. Kottam, and S. P. Smrithi, "Carica-Papaya derived Carbon nanodots for the detection of Fe(III) ions," *Applied Science and Engineering Progress*, vol. 18, Art. No. 7571, 2025. doi: 10.14416/j.asep.2024.09.005.